Chemical Methodologies 7(2023) 314-324

Chemical Methodologies

Journal homepage: http://chemmethod.com

*Original Research Article*

# A Novel Design for Gas Sensor of Zinc Oxide Nanostructure Prepared by Hydrothermal Annealing Technique

**Ali E. Hashim*, Fuad T. Ibrahim**

*University of Baghdad, College of Science, Department of physics, Baghdad, Iraq*

**ARTICLE INFO**

**Article history**

Submitted: 2022-10-25
Revised: 2022-11-31
Accepted: 2022-12-31
Manuscript ID: CHEMM-2212-1634
Checked for Plagiarism: Yes
Language Editor:
Dr. Fatimah Ramezani
Editor who approved publication:
Dr. Abdolkarim Zare

**DOI**:10.22034/CHEMM.2023.377977.1634

**KEYWORDS**

Zn
Structural Properties
Optical Properties
FE-SEM
Gas Sensing

**ABSTRACT**

Zinc oxide (ZnO) nanoparticles were prepared under different conditions using hydrothermal technique. The effect of reaction time on the size and shape of the nanoparticles was studied. It was evident that with the increase in the reaction time, the size of the granules shrank and the nanotubes were formed in the FESEM image, appeared as cubes and nano-spheres. The ZnO powder had polycrystalline structure with (101) peaks in the diffraction spectrum, as indicated by the X-ray spectra. The UV spectrum showed variation in the band gap due to the different sizes of the nanoparticles. The properties of the zinc oxide for hydrogen sulfide ($H_2S$) gas were studied as a function of temperature and change in time under the optimal lab conditions. The sensitivity, response time, and recovery time were calculated with operating temperatures. The results showed that the sensitivity had higher increase with raising the operating temperature. The maximum sensitivity of the tested gas sensor at 50 ppm of $H_2S$ was about 1098 % at around 200 °C for 1 hour. It was found that the lowest response time was at 100 °C for 1 hour, and the response time was 8 s.

**GRAPHICAL ABSTRACT**

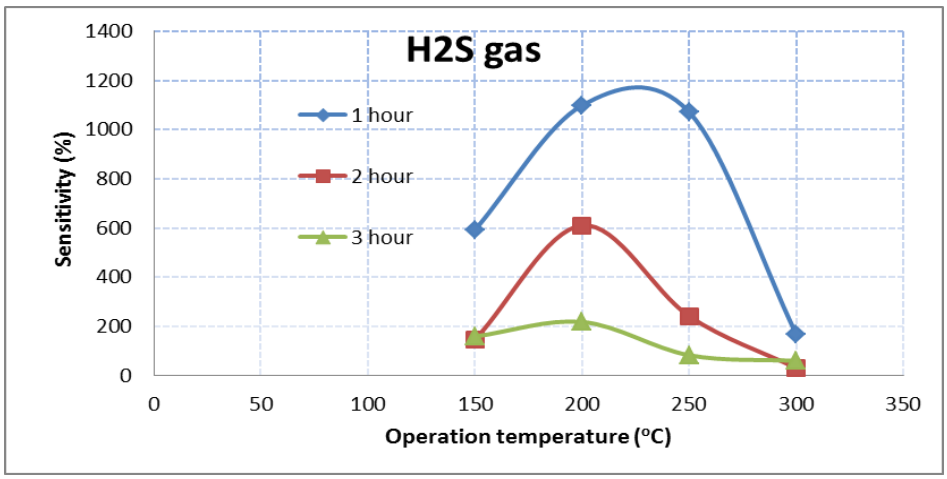


* Corresponding author: Ali E. Hashim
✉ E-mail: ali.ihsan1204a@sc.uobaghdad.edu.iq

## Introduction

Several techniques have been used up to this point to create the ZnO material as a variety of one-dimensional nanostructure forms, such as nanowires, nanorods, and superstructures such as nanotubes, filaments, and nanocrystals [1-4]. They stand for a large range of nanoscale components assembled into useful devices such those with short and acoustic wavelengths, lasers, photodetectors, gas sensors, solar cells, piezoelectric transducers, and actuators [5]. There are numerous ways to create ZnO nanostructures, including sol-gel method, vapour transport process, vapour-solid process (VS), vapour-liquid-solid process (VLS), epitaxial electrodeposition (ED), and metal-organic chemical reactions such as aqueous chemical procedures, MOCVD, PLD, and hydrothermal methods. On the other hand, hydrothermal procedures have numerous benefits, including low cost, simplicity of use, efficiency of energy use, and scalability, and as a result, have recently noticed for the creation of one-dimensional nanostructures [6, 7]. There is a growing need for better gas sensors with higher sensitivity and selectivity [8, 9], and thus great efforts have been put into developing these technologies. In search of better nanomaterials for sensing, ZnO and $TiO_2$ are examples of semiconductor metal oxides (MOS). The wide range of researches has been done on tungsten oxide ($WO_3$) and other materials for applications such as gas sensing. Seiyama *et al.* (1962) were the first who examined gas sensing capabilities of ZnO-based gas sensor. Due to its high carrier mobility of conduction electrons, good chemical, and thermal stability, direct wide bandgap (e.g., 3.37 eV), and a large excitation binding energy (60 meV), ZnO has gained an important status in various MOS nanomaterials [10]. ZnO structure and morphology, including its surface area, size, orientation, and crystal density have a significant impact on its gas-detecting abilities [11]. Therefore, it is crucial to customize ZnO structure and morphology to maximize its gas sensing capability. This can be accomplished, in particular, by complicated design of special three-dimensional hierarchical architectures that have high surface areas, quick gas diffusion, and a reduced agglomeration of low-dimensional structures. The large range of applications of ZnO-based gas sensors is restricted by their typical drawbacks of sluggish response, poor selectivity, and lack of long-term stability to obtain a trustworthy and effective dissolution [12]. This study was focused on two, one through hydrothermal approach to create ZnO nanostructures, and looking into the effects of the processing time. The second was focused on demonstrating sensitivity, response time and recovery time of the prepared samples with the operation temperature, to enhance these sensors ZnO characteristics and its gas detection system.

## Materials and Methods

A mass of 4 g of zinc chloride ($ZnCL_2$) as a powder was diluted in 100 ml of distilled water and stirred for 30 min. Next, ammonia hydroxide ($NH_4OH$) pellets was dropped on the former zinc chloride solution until the reactants pH hits 12. The solution was blended, and then put into Teflon-lined and hermetically sealed stainless steel autoclaves. After that, the solution was kept in a hydrothermal oven for l, 2, and 3 hours, at 150 °C. The outcome was filtered by centrifuge, after being cooled at room temperature, and then it was put in a container to dry in the oven after being rinsed with distilled water. After that the resultant was a non-dried power placed on a slice in the oven to be dried at 40 °C. Thereafter, the dried powder was mixed again with distilled water to be liquid and precipitated on a glass slide as a film. Then, the film was connected to electrodes to be examined in the system, as a gas sensor. There were the electrical feeds through the base plate. The heating was varied on the base plate to heat the sample under test to obtain required operating temperatures. The current passing through the heating element was monitored using a relay with adjustable ON/OFF time intervals. A thermocouple was used to sense the operating temperature of the sensors. The output of the thermocouple was connected to digital temperature indicators. A gas inlet valve

was fitted at one port of the base plate. The required gas concentration inside the system was achieved by injecting known volume of test gas using a gas flow meter. A constant voltage was applied to the sensors, and the current was measured by a digital millimeter. Air was allowed to pass into the chamber after every gas exposure cycle.

*Characterization detail*

The morphology of the samples was examined using FE-SEM inspect (F50-FE company). X-ray diffraction technique (6000 SHIMADZ- Japan) was used to measure the average crystallite size and crystal structure. A spectrophotometer (Lambda 365 Perkin Elme) with a spectrum range of 190-1100 nm double beam was used to measure the UV absorption.

## Results and Discussion

*X-Ray diffraction of ZnO powder*

Figure 1a, b, and c shows the XRD diffraction patterns of the ZnO powder at different time periods 60, 120, and 180 min at constant temperature 150 °C, that were prepared by hydrothermal method. It appears from the X-ray spectrum that the ZnO powder has a polycrystalline structure with 13 peaks in the diffraction spectrum which are (100), (002), (101), (102), (110), (103), (200), (112), (112), (201), and (202) corresponding to the JCPDS data (JCPDS card No. 79-0207) which refers to a hexagonal [13, 14] structure. Tables 1, 2 and 3 show the results of the XRD diffraction patterns. The crystal size was calculated using the Scherrer equation [15].

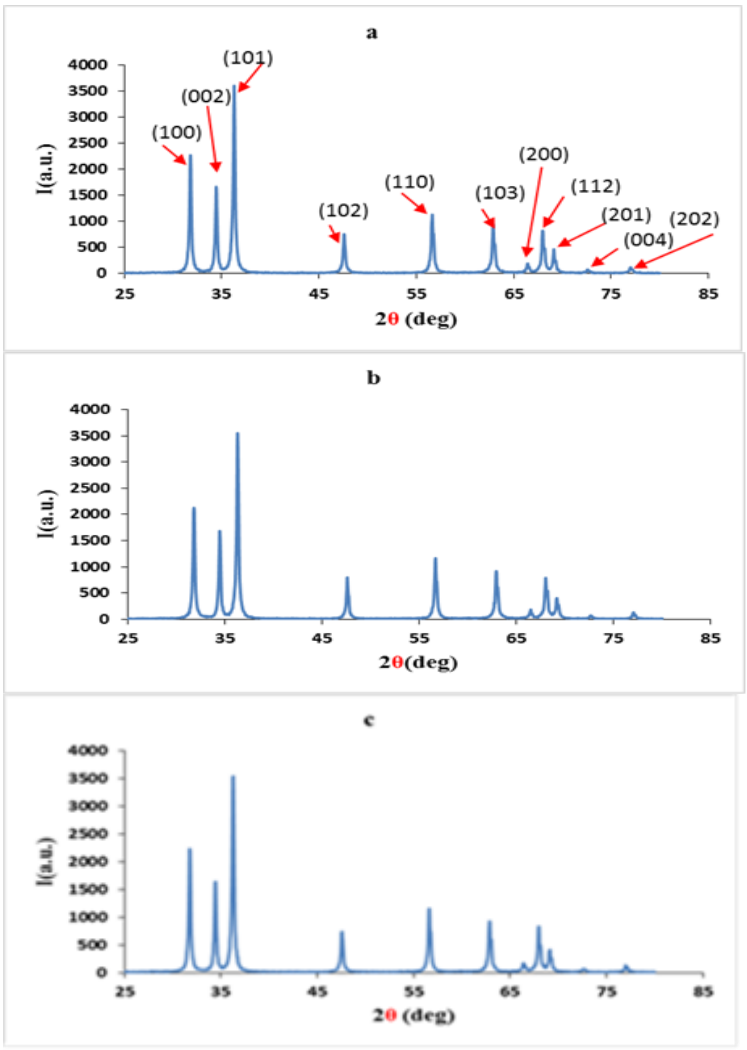


**Figure 1:** XRD diffraction of ZnO powder: (a) 60 min, (b) 120 min, and (c) 180 min, at 150 °C

**Table 1:** XRD characterization for ZnO powder (a) at 60 min

| *2 θ (deg)* | *d observed (Å)* | *FWHM (deg)* | *D (nm)* | *δ × $10^{14}$lines.$m^{-2}$* | *η ×$10^{-4}$lines$^{-2}$.$m^{-4}$* |
|---|---|---|---|---|---|
| 31.8 | 2.81 | 0.21 | 69.62 | 4.97 | 2.06 |
| 34.4 | 2.59 | 0.21 | 69.62 | 4.97 | 2.06 |
| 36.2 | 2.47 | 0.21 | 69.62 | 4.97 | 2.06 |
| 47.6 | 1.90 | 0.22 | 66.46 | 5.21 | 2.26 |
| 56.6 | 1.62 | 0.20 | 73.10 | 4.73 | 1.87 |
| 62.8 | 1.47 | 0.21 | 69.62 | 4.97 | 2.06 |
| 66.4 | 1.40 | 0.22 | 66.46 | 5.21 | 2.26 |
| 68.8 | 1.37 | 0.14 | 104.44 | 3.31 | 0.91 |
| 69.2 | 1.35 | 0.21 | 69.62 | 4.97 | 2.06 |
| 73.4 | 1.29 | 0.22 | 66.46 | 5.21 | 2.26 |
| 77 | 1.23 | 0.23 | 63.57 | 5.45 | 2.47 |

**Table 2:** XRD characterization for ZnO powder (b) at 120 min

| *2 θ (deg)* | *d observed (Å)* | *FWHM (deg)* | *D (nm)* | *δ × $10^{14}$lines.$m^{-2}$* | *η ×$10^{-4}$lines$^{-2}$.$m^{-4}$* |
|---|---|---|---|---|---|
| 31.8 | 2.80 | 0.22 | 66.46 | 5.21 | 2.26 |
| 34.4 | 2.59 | 0.21 | 69.62 | 4.97 | 2.06 |
| 36.3 | 2.47 | 0.21 | 69.62 | 4.97 | 2.06 |
| 47.6 | 1.90 | 0.20 | 73.10 | 4.73 | 1.87 |
| 56.6 | 1.62 | 0.21 | 69.62 | 4.97 | 2.06 |
| 62.9 | 1.47 | 0.22 | 66.46 | 5.21 | 2.26 |
| 66.6 | 1.40 | 0.22 | 66.46 | 5.21 | 2.26 |
| 68 | 1.37 | 0.22 | 66.46 | 5.21 | 2.26 |
| 69.1 | 1.35 | 0.22 | 66.46 | 5.21 | 2.26 |
| 72.5 | 1.29 | 0.20 | 73.10 | 4.74 | 1.87 |
| 77.2 | 1.23 | 0.21 | 69.62 | 4.98 | 2.06 |

**Table 3**: XRD characterization for ZnO powder (c) at 180 min

| *2θ (deg)* | *d observed (Å)* | *FWHM (deg)* | *D (nm)* | *δ × $10^{14}$lines.$m^{-2}$* | *η ×$10^{-4}$lines$^{-2}$.$m^{-4}$* |
|---|---|---|---|---|---|
| 31.7 | 2.81 | 0.21 | 69.62 | 4.98 | 2.06 |
| 34.4 | 2.60 | 0.21 | 69.62 | 4.97 | 2.06 |
| 36.2 | 2.47 | 0.22 | 66.46 | 5.21 | 2.26 |
| 47.5 | 1.91 | 0.16 | 91.38 | 3.79 | 1.19 |
| 56.6 | 1.62 | 0.21 | 69.62 | 4.97 | 2.06 |
| 62.8 | 1.47 | 0.22 | 66.46 | 5.21 | 2.26 |
| 66.4 | 1.40 | 0.20 | 73.10 | 4.73 | 1.87 |
| 68.0 | 1.37 | 0.21 | 69.62 | 4.97 | 2.06 |
| 69.2 | 1.35 | 0.22 | 66.46 | 5.21 | 2.26 |
| 72.8 | 1.29 | 0.21 | 69.62 | 4.97 | 2.06 |
| 77.1 | 1.23 | 0.20 | 73.10 | 4.73 | 1.87 |

*Scanning electron microscope of ZnO*

Figure 2a, b, and c shows the SEM images of the ZnO powder prepared with hydrothermal method and different SEM images which confirm different morphologies of these particles. The morphology of these particles consists of relatively uniform and smooth surface rod-like micro-structures had an average particle size of (122.01), (316.6) nm, and (6.098) μm at different time periods of 60, 120, and 180 min, respectively. This result was agreed with N. D. Dien [16].

*Optical properties (UV-Visible spectroscopy)*

Figure 3 displays the absorbance spectra of the ZnO colloidal in a range of 200-1100 nm that were prepared by hydrothermal method. It was observed that the ZnO nanoparticles have their absorption peaks at 387 nm. The absorption peak shows a red shift compared with that of bulk ZnO (365 nm) [17]. It was also observed that all the samples tend to red shift can be attributed to the development of shallow levels inside the band gap due to the presence of foreign atoms in the lattice [18]. The shift of the absorption peak to higher wavelength indicated the decrease in the optical band gap.

Figure 4 demonstrates the reflectance spectrum of ZnO at different period times as a function of wavelength in range of 200-1100 nm. It was found that the reflectivity decreased with increasing time to record 0.06, 0.19, and 0.2 at different time periods of 60, 120, and 180 min, respectively, at wavelength of 200 nm.

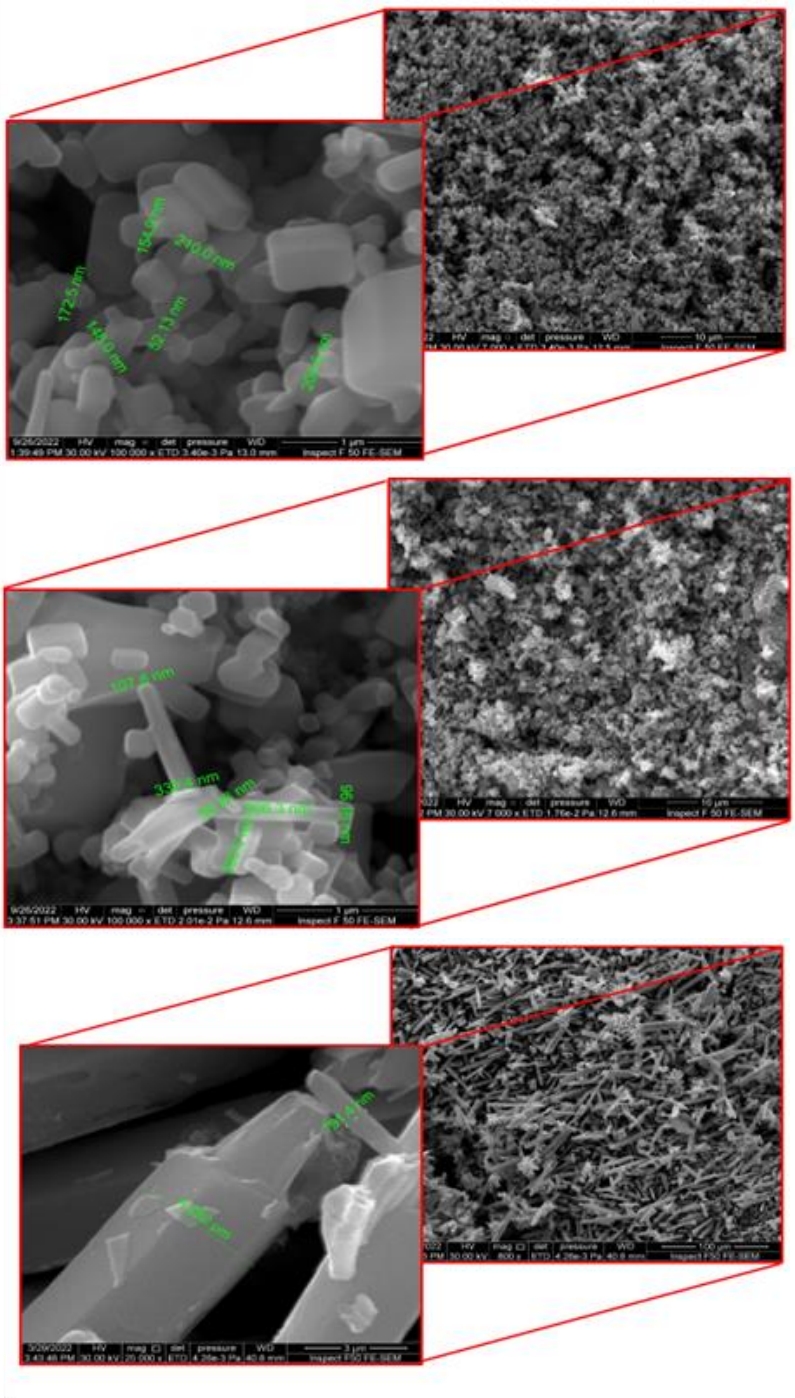

**Figure 2:** FE-SEM images of ZnO at different time periods: (a) 60 min, (b) 120 min and (c) 180 min, at 150 °C

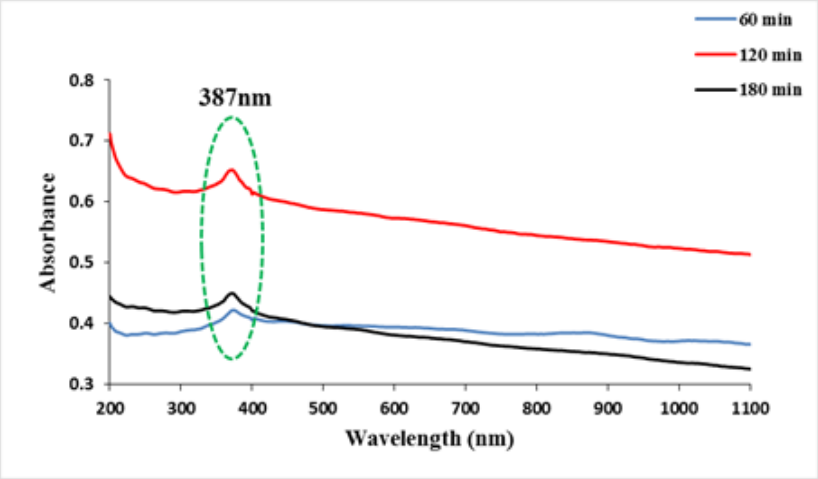


**Figure 3:** UV-Visible spectra of ZnO NPs at different time periods: (a) 60 min, (b) 120 min, and (c) 180 min, at 150 °C

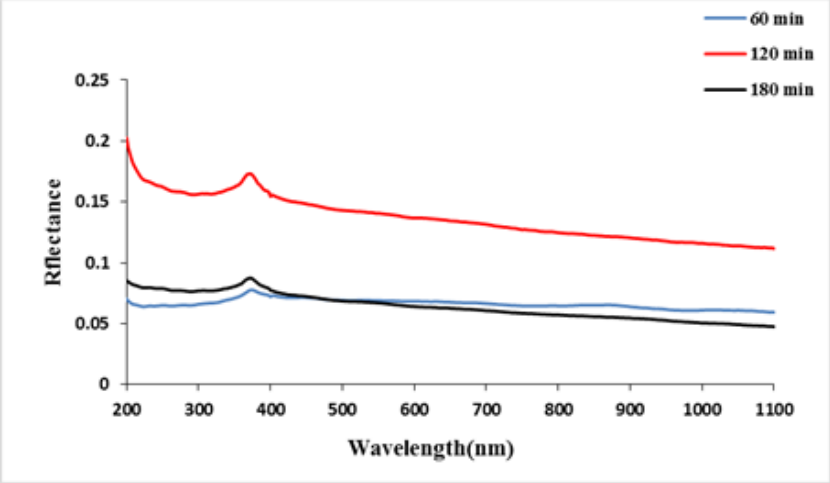


**Figure 4:** Reflectance spectra of ZnO NPs at different time periods: (a) 60 min, (b) 120 min, and (c) 180 min, at 150 °C

The refractive index is an important parameter for semiconductor materials and applications, and it can be calculated from the following relationship:

$$n = \frac{1+R^{0.5}}{1-R^{0.5}} \qquad (1)$$

The refractive index, as a function of the reflectivity (R), depends on several factors including type of the material and the crystal structure. The refractive index values are varied depending on the change of roughness of the samples surface. Table 4 presents the change in the refractive index of ZnO at different time periods where it was found that the maximum values were 1.7, 2.4, and 1.8. High refractive index materials can be used in many optoelectronic applications [19, 20].

Tauc equation was applied by plotting the $(\alpha h\nu)^2$ versus photon energy ($h\nu$) and extrapolation of the linear portion of the curve to absorption is equal to zero, as listed in Table 2 [21], while the energy gap of ZnO at different time periods was found to be 3.3, 3.4, and 3.2 eV at different time periods of 60, 120, and 180 min, respectively.

*Gas sensing measurement*

Figure 5 illustrates the sensitivity as a function of operating temperature in range of 150-300 °C for the prepared ZnO with different preparation times, that were deposited on glass substrates at 10% of $H_2S$:air mixing ratio on the all the samples.

**Table 4:** Refractive index and photon energy of ZnO at different time periods: (a) 60 min, (b) 120 min, and (c) 180 min, at 150 °C

| Sample | Eg (eV) | N |
|---|---|---|
| 60 min | 3.4 | 1.7 |
| 120 min | 3.3 | 1.8 |
| 180 min | 3.2 | 2.4 |

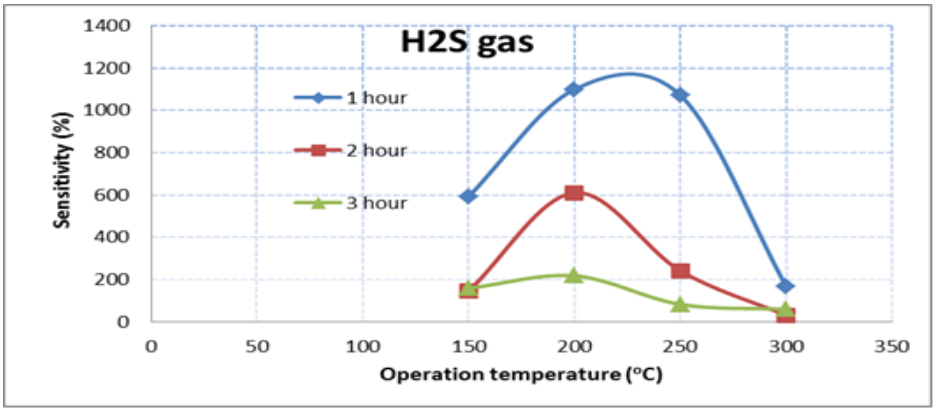


**Figure 5:** Sensitivity vs. operating temperature of the ZnO using $H_2S$ as gas sensing technique

The effect of the operation temperature on the thin film sensitivity was studied with the aim of optimizing of the operation temperature to the lowest possible value. The operating temperature is defined as the temperature at which the resistance of the sensor reaches a constant value. The changing of resistance is just only influenced by the presence of amount of some gases of interest [22, 23]. The results showed that the sensitivity had higher increase with increasing of the operating temperature. The maximum sensitivity of the tested gas sensor to 50 ppm for $H_2S$ was about 1098% at around 200 °C for 1 hour preparation sample, while 3 hours preparation sample, gas sensor had 58% lowest sensitivity for $H_2S$ gas. It was noted that the optimum sensing temperature required for the maximum sensitivity was around 200 °C for all the samples. All the above results showed that the sensitivity of the oxidizing and reducing gases was greatly enhanced. The reason can be attributed to the nano-sized ZnO particle on the glass substrate and the increased amount of surface adsorbed oxygen species.

Figures 6 and 7 indicate the relationship between the response time and the recovery time with operating temperature. Figure 6 shows that the response time with rising operating temperature for $H_2S$ test gas, where the response time decreased with increasing the operating temperature. The fast response speed for $NO_2$ gas was 9.9 sec for 1 h sample at 200 °C. Figure 7 shows that the recovery time with rising operating temperature for $H_2S$ test gas decreased with increasing the operating temperature. The fast recover speed for $H_2S$ gas was 50.4 s for 3 hours of the ZnO sample at 300 °C. The particular decrease with work function and the activation energy of surface reaction may be associated with decreasing grain size and an increase in vacancies created upon SiC lattice [24].

The increase in the adsorption of oxygen on the surface extracts conduction electrons from the near surface region forming an electron depleted surface layer. This increase in the number of active adsorption sites effects on the fast response time for sensors. Generally, the response time and recovery time were decreased with increasing the operation temperature, as shown in figures. In real situations, a fast response time is usually required, as well as, fast recovery time. Figure 8 depicts the variation of resistance with time for the ZnO prepared samples as exposed to 10 % $H_2S$ gas in the air ambient injected into testing chamber and bias voltage at 3V, at optimal operating temperature of each sample.

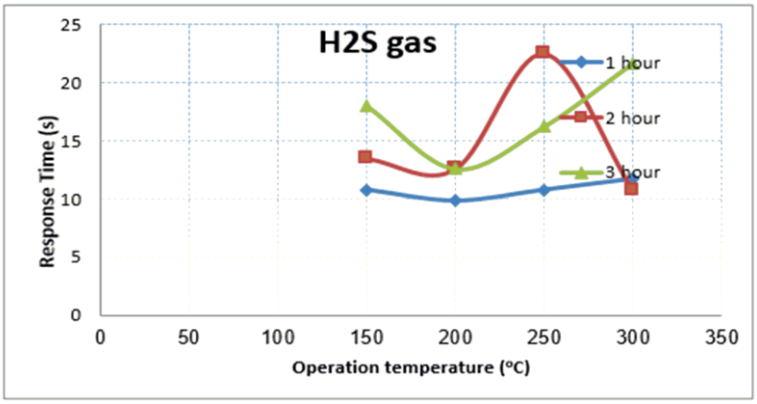


**Figure 6:** Response time vs. operation temperature of the ZnO gas sensor using $H_2S$ gas

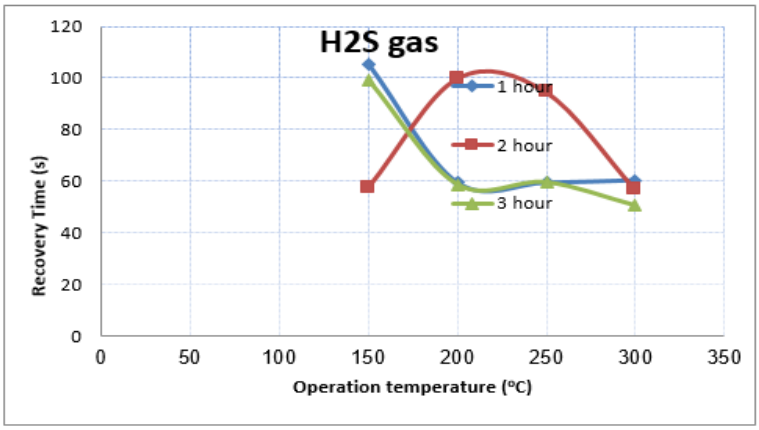


**Figure 7:** Recovery time vs. operation temperature of the ZnO gas sensor using $NH_3$ gas

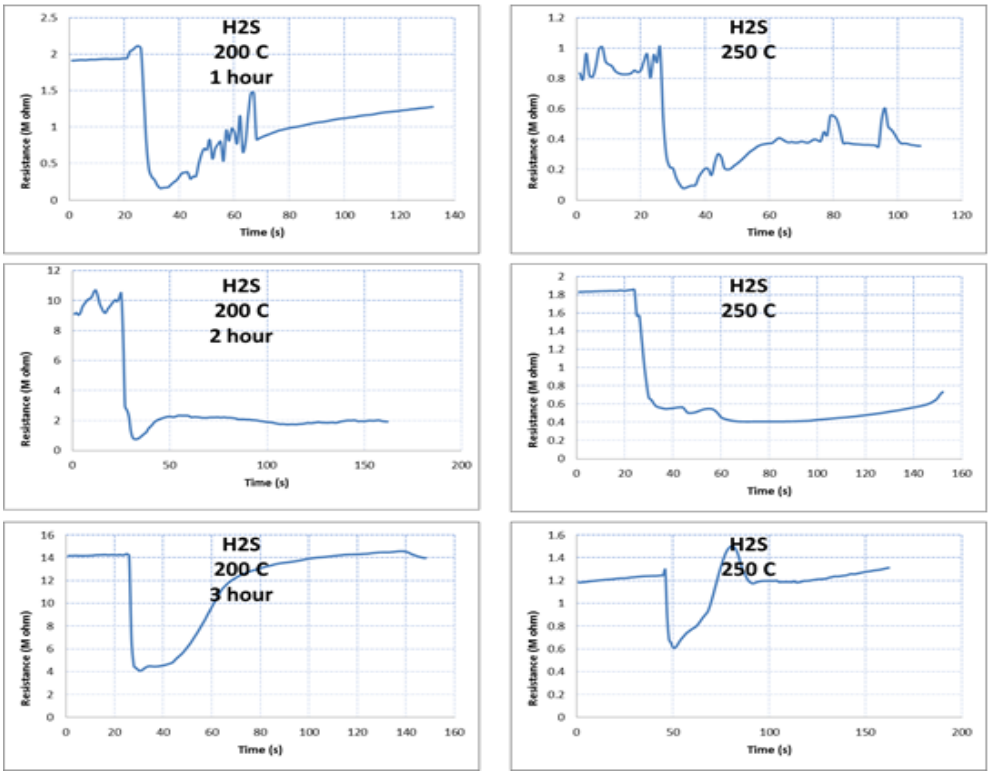


**Figure 8.** The variation resistance with time for different operation temperatures of $H_2S$ gas for the ZnO gas sensor

The resistance was measured directly with time and the sensor resistance initially reached the steady state before gas opening. In this time, the gas would open to allow mixing with air inside the chamber. The resistance was decreased abruptly to reach a steady state, and then the gas was switched off. After that the electrical resistance returned to the initial case. The ability of a sensor to sense the presence of gas depends on the nature of the interaction between the gas molecules and the surface atoms of the sensing film. Figure 8 shows that the resistance of the samples decreased with exposing $H_2S$ gas on the surface. The behaviour of the samples indicated that ZnO have higher sensitivity and selectivity for $H_2S$ reducing gas specially at 200 °C.

Table 5 indicates gas sensor parameters and the results obtained in this research were compared with the results obtained previously, as they were compatible with them [25, 26].

**Table 5:** Gas sensor parameters

| Operation temperatures | Time periods (h) | Response time (s) | Recovery time (s) | Sensitivity (%) |
|---|---|---|---|---|
| 150 | 1 | 11 | 105 | 600 |
| | 2 | 13 | 60 | 200 |
| | 3 | 17 | 98 | 200 |
| 200 | 1 | 10 | 60 | 1100 |
| | 2 | 12.5 | 100 | 600 |
| | 3 | 12.5 | 60 | 200 |
| 250 | 1 | 11 | 60 | 1050 |
| | 2 | 25 | 98 | 200 |
| | 3 | 16 | 60 | 100 |
| 300 | 1 | 12 | 60 | 200 |
| | 2 | 11 | 60 | 50 |
| | 3 | 22 | 50 | 50 |

## Conclusion

This study was clearly demonstrated the process of the production of ZnO thin films. The accompanying graphs of the ZnO particle dynamics illustrated this film. They showed signs of $H_2S$ with improved sensitivity, faster response, and slower recovery time of the sensors. The hydrothermal method is the best method for preparing zinc oxide because it contains no by-products, economically feasible, and does not produce fumes or toxic substances that are difficult to remove. It was also showed that increasing the reaction time by no more than 2 hours leads to an increase in the incident rays in the longest UV wavelength range. It can be concluded that the large increase in the energy gap was due to the effect of the quantum size, and the amount of the energy gap qualifies the material to be a large effective medium in ultraviolet photodetectors. The FSEM results demonstrated that the surface has a nanostructure and that nanoparticles of average size were present.

## Funding

This research did not receive any specific grant from funding agencies in the public, commercial, or not-for-profit sectors.

## Authors' contributions

All authors contributed to data analysis, drafting, and revising of the paper and agreed to be responsible for all the aspects of this work.

## Conflict of Interest

We have no conflicts of interest to disclose.

## Orcid

*Ali E. Hashim*
https://orcid.org/0000-0002-0269-2325
*Fuad T. Ibrahim*
https://orcid.org/0000-0001-9796-9990

## References


[1]. Fan Z., Lu, J.G., Zinc oxide nanostructures: synthesis and properties, *Journal of nanoscience and nanotechnology*, 2005, **5**:1561 [Crossref], [Google scholar], [Publisher]

[2]. Xie S., Xia Y., Zheng Z., Zhang X, Yuan J., Zhou H., Zhang Y. Effects of Nonradiative Losses at Charge Transfer States and Energetic Disorder on the Open-Circuit Voltage in Nonfullerene Organic Solar Cells, *Advanced Functional Materials*, 2018, **28**:1705659 [Crossref], [Google scholar], [Publisher]

[3]. Gao T., Li Q., Wang T., Sonochemical Synthesis, Optical Properties, and Electrical Properties of Core/Shell-Type ZnO Nanorod/CdS Nanoparticle Composites. *Chem. Mater.*, 2005, **17**:887 [Crossref], [Google scholar], [Publisher]

[4]. Xi G., Peng Y., Yu W., Qian Y., Synthesis, Characterization, and Growth Mechanism of Tellurium Nanotubes, *Crystal Growth & Design*, 2005, **5**:935 [Crossref], [Google scholar], [Publisher]

[5]. Baranov A.N., Chang C.H., Shlyakhtin O.A., Panin G.N., In situ study of the ZnO–NaCl system during the growth of ZnO nanorods, *Nanotechnology*, 2004, **15**:1613 [Crossref], [Google scholar], [Publisher]

[6]. Zhang Y., Ram M.K., Stefanakos E.K., Goswami D.Y., "Synthesis, Characterization, and Applications of ZnO Nanowires," *Journal of Nanomaterials*, 2012, **2012**:1 [Crossref], [Google scholar], [Publisher]

[7]. Lai Y., Meng M., Yu Y., Wang X., Ding T., Photoluminescence and photocatalysis of the flower-like nano-ZnO photocatalysts prepared by a facile hydrothermal method with or without ultrasonic assistance, *Applied Catalysis B: Environmental*, 2011, **105**:335 [Crossref], [Google scholar], [Publisher]

[8]. Sun Y.F., Liu S.B., Meng F.L., Liu J.Y., Jin Z., Kong L.T., Metal oxide nanostructures and their gas sensing properties: a review, *Sensors*, 2012, **12**:2610 [Crossref], [Google scholar], [Publisher]

[9]. Gardon M., Guilemany J.M., A review on fabrication, sensing mechanisms and performance of metal oxide gas sensors, *Journal of Materials Science: Materials in Electronics*, 2013, **24**:1410 [Crossref], [Google scholar], [Publisher]

[10]. Ganesh R.S., Durgadevi E., Navaneethan M., Patil V.L., Ponnusamy S., Muthamizhchelvan C., Kawasaki S., Patil P.S., Hayakawa Y., Low temperature ammonia gas sensor based on Mn-doped ZnO nanoparticle decorated microspheres, *Journal of Alloys and Compounds*, 2017, **721**:182 [Crossref], [Google scholar], [Publisher]

[11]. Cho S., Kim S., Jung D.W., Lee K.H., Formation of quasi-single crystalline porous ZnO nanostructures with a single large cavity, *Nanoscale*, 2011, **3**:3841 [Crossref], [Google scholar], [Publisher]

[12]. Wang X., Liu W., Liu J., Wang F., Kong J., Qiu S., He C., Luan L, *ACS Appl. Mater. Interfaces*, 2012, **4**:817. [Crossref], [Google scholar], [Publisher]

[13]. Pascariu P., Homocianu M., Cojocaru C., Samoila P., Airinei A., Suchea M. Preparation of La doped ZnO ceramic nanostructures by electrospinning–calcination method: Effect of La3+ doping on optical and photocatalytic properties. *Applied Surface Science*, 2019, **476**:16 [Crossref], [Google scholar], [Publisher]

[14]. Muhammad W., Ullah N., Haroon M., Abbasi B.H., Optical, morphological and biological analysis of zinc oxide nanoparticles (ZnO NPs) using Papaver somniferum L., *RSC advances,* 2019, **9**:29541 [Crossref], [Google scholar], [Publisher]

[15]. Scherrer P., Nachrichten von der Gesellschaft der Wissenschaften zu Göttingen, Mathematisch-Physikalische Klasse, *Göttinger Nachrichten Gesell.*, 1918, **2**:98 [Publisher]

[16]. Dien N.D., Preparation of various morphologies of ZnO nanostructure through wet chemical methods. *Advanced Materials Science*, 2019, **4**:1 [Crossref], [Google scholar], [Publisher]

[17]. Girish Y.R., Kumar K.S.S., Manasa H.S., Shashikanth S. ZnO: An Ecofriendly, Green Nano-catalyst for the Synthesis of Pyrazole Derivatives under Aqueous Media. *Journal of the Chinese Chemical Society*, 2014, **61**:1175 [Crossref], [Google scholar], [Publisher]

[18]**.** Sun J.H., Dong S.Y., Feng J.L., Yin X.J., Zhao X.C., Enhanced sunlight photocatalytic performance of Sn-doped ZnO for Methylene Blue degradation, *Journal of Molecular Catalysis A:*

*Chemical*, 2011, **335**:145 [Crossref], [Google scholar], [Publisher]
[19]. Yen H.J., Liou G.S., Enhanced near-infrared electrochromism in triphenylamine-based aramids bearing phenothiazineredox centers, *J. Mater. Chem*., 2010, **20**:408 [Crossref], [Google scholar], [Publisher]
[20]. Macdonald E.K., Shaver M., Intrinsic high refractive index polymers, *Polym. Int.*, 2015, **64**:6 [Crossref], [Publisher]
[21]. Varshni Y.P., Temperature dependence of the energy gap in semiconductors, *Physica*, 1967, **34**:149 [Crossref], [Google scholar], [Publisher]
[22]. Karunagaran B., Uthirakumar P., Chung S.J., Velumani S., Suh E.K., $TiO_2$ thin film gas sensor for monitoring ammonia, *Materials Characterization*, 2007, **58**:680 [Crossref], [Google scholar], [Publisher]
[23]. Korotcenkov G., Metal oxides for solid-state gas sensors: What determines our choice?, *Materials Science and Engineering: B*, 2007, **139**:1 [Crossref], [Google scholar], [Publisher]
[24]. Vanalakar S.A., Agawane G.L., Shin S.W., A review on pulsed laser deposited CZTS thin films for solar cell applications, *Journal of Alloys and Compounds*, 2015, **619**:109 [Crossref], [Google scholar], [Publisher]
[25]. Aleksanyan M., Sayunts A., Shahkhatuni G., Simonyan Z., Kasparyan H., Kopecký D. *Nanomaterials*, 2023, **13**:120 [Crossref], [Google scholar], [Publisher]
[26]. Hsueh T.J., Ding R.Y., A Room Temperature ZnO-NPs/MEMS Ammonia Gas Sensor, *Nanomaterials*, 2022, **12**:3287 [Crossref], [Google scholar], [Publisher]

**HOW TO CITE THIS ARTICLE**
Ali E. Hashim, Fuad T. Ibrahim. A Novel Design for Gas Sensor of Zinc Oxide Nanostructure Prepared by Hydrothermal Annealing Technique. *Chem. Methodol.*, 2023, 7(4) 314-324
**DOI**: https://doi.org/10.22034/CHEMM.2023.377977.1634
URL: http://www.chemmethod.com/article_164845.html